

Oleg P. Korobeinichev, Ilya E. Gerasimov, Denis A. Knyazkov, Andrey G. Shmakov, Tatyana A. Bolshova, Nils Hansen, Charles K. Westbrook*, Guillaume Dayma, and Bin Yang

An Experimental and Kinetic Modeling Study of Premixed Laminar Flames of Methyl Pentanoate and Methyl Hexanoate

Abstract: Detailed chemical structures of stoichiometric and rich premixed laminar flames of methyl pentanoate and methyl hexanoate were investigated over a flat burner at 20 Torr and for methyl pentanoate at 1 atm. Molecular beam mass spectrometry was used with tunable synchrotron vacuum ultraviolet (VUV) photoionization for low pressure flames of both methyl pentanoate and methyl hexanoate, and soft electron-impact ionization was used for atmospheric pressure flames of methyl pentanoate. Mole fraction profiles of stable and intermediate species, as well as temperature profiles, were measured in the flames. A detailed chemical kinetic high temperature reaction mechanism for small alkyl ester oxidation was extended to include combustion of methyl pentanoate and methyl hexanoate, and the resulting model was used to compare computed values with experimentally measured values. Reaction pathways for both fuels were identified, with good agreement between measured and computed species profiles. Implications of these results for future studies of larger alkyl ester fuels are discussed.

Keywords: Spectroscopy, Reaction Kinetics.

DOI 10.1515/zpch-2014-0596

Received August 29, 2014; accepted December 15, 2014

Dedicated to Professor Henning Bockhorn on the occasion of his 70th birthday

***Corresponding author: Charles K. Westbrook**, Lawrence Livermore National Laboratory, Livermore, CA, USA, e-mail: westbrookck@earthlink.net

Oleg P. Korobeinichev, Ilya E. Gerasimov, Tatyana A. Bolshova: Institute of Chemical Kinetics and Combustion, Novosibirsk, Russia

Denis A. Knyazkov, Andrey G. Shmakov: Institute of Chemical Kinetics and Combustion, Novosibirsk, Russia; and Novosibirsk State University, Novosibirsk, Russia

Nils Hansen: Sandia National Laboratories, Livermore, CA, USA

Guillaume Dayma: Centre National de la Recherche Scientifique, Orleans Cedex 1, France

Bin Yang: Center for Combustion Energy, Tsinghua University, Beijing, China

1 Introduction

Interest in fuels derived from biomass has emerged due to decreasing availability of petroleum-based fuels, as well as concerns about CO₂ production and the potential of renewable fuels. Addressing these issues as well as improving the performance of internal combustion engines running on biodiesel fuel requires knowledge of the combustion chemistry of that fuel. The main objective of the current project is to refine biodiesel combustion kinetic models based on experimental studies and computer simulations.

One important class of biofuels consists of vegetable oils that have been processed by trans-esterification to make “biodiesel fuel”, alkyl esters of the desired molecular size and combustion characteristics to be viable diesel fuels [1–3]. These fuels have Cetane Numbers (CN) comparable with those of conventional, petroleum-based diesel fuels and generally perform well in conventional diesel engines. However, some biodiesel combustion properties are somewhat different from those of conventional diesel fuels, such as somewhat lower soot production [4], possibly higher NO_x production [5], and somewhat anomalous early production of CO₂ from biodiesel combustion, and these differences have been related to the fact that biodiesel fuel molecules have a terminal alkyl ester group that has subtle effects on chemical kinetics of its combustion.

While many of these differences in combustion kinetics between conventional and biodiesel fuels have been answered, other questions remain. In particular, flame propagation kinetics of biodiesel fuels have not been studied in any detail. One reason for this apparent oversight is that biodiesel molecules are very large molecules, largely the saturated components methyl stearate (C₁₉H₃₈O₂) and methyl palmitate (C₁₇H₃₄O₂), the singly unsaturated methyl oleate (C₁₉H₃₆O₂), doubly unsaturated methyl linoleate (C₁₉H₃₄O₂) and triply unsaturated methyl linolenate (C₁₉H₃₂O₂). Because of the large number of heavy atoms in these molecules and their intermediate products, kinetic reaction mechanisms for combustion of these fuels are extremely large and simulations using them are computationally quite expensive. For example, the biodiesel kinetic model for soy and rapeseed biodiesel fuels by Westbrook et al. [6, 7] included more than 5000 individual chemical species and 20,000 elementary reactions. Ignition kinetics and combustion in homogeneous stirred reactors of these very large compounds have been studied in a number of recent publications [6–15], but those studies treated only spatially homogeneous problems, and a huge increase in dimensionality is encountered in problem size when even a one-dimensional problem like a premixed laminar flame is posed. Of course, much of the complexity of such kinetic mechanisms comes from the low temperature, alkylperoxy radical isomer-

ization kinetics, and those low temperature submechanisms are generally not required for simulations of laminar flames, but even the high temperature submechanisms for real biodiesel fuels are often prohibitively large. As a result, detailed kinetic solutions for laminar biodiesel fuel flames have not yet been reported. The present study explores the computational challenges involved in stretching current 1D, spatially varying simulations to methyl ester fuels larger than methyl butanoate.

There is a continuing need to examine how the terminal methyl ester moiety present in biodiesel fuel molecules influences the laminar flame kinetics, and the most successful strategy has been to study laminar flames of methyl and ethyl esters that are much smaller than the C_{18} and C_{16} methyl esters found in biodiesel fuel. Laminar flame simulations have been carried out previously for low pressure premixed flames of small alkyl ester fuels, including methyl formate, methyl acetate, methyl propanoate, methyl propenoate, methyl butanoate, methyl crotonate, methyl isobutanoate, as well as ethyl formate, ethyl acetate, ethyl propanoate, ethyl propenoate, and vinyl acetate [16–18], all of which have studied in particular the kinetic effects of the alkyl ester group and how HOCO and CH_3OCO radicals affect pyrolysis and flame propagation. Recent theoretical studies [19–23] have examined the reaction pathways of these HOCO and CH_3OCO species in methyl ester fuels. Other kinetic reaction mechanisms have been developed recently by Dayma et al. [24–27] for opposed flow diffusion flames and jet-stirred reactor experiments of methyl hexanoate, methyl heptanoate, methyl octanoate, and ethyl pentanoate. In another recent study, Glaude et al. [28] developed kinetic mechanisms to describe the homogeneous oxidation of methyl hexanoate, methyl heptanoate, and methyl decanoate at low temperatures in a jet-stirred reactor. The present study contributes new experimental laminar flame species measurements for both methyl pentanoate and methyl hexanoate, and the combination of experimental results for both fuels in common experimental facilities makes it possible to inter-compare the laminar flame properties of both fuels.

The present work provides new experimental results for low pressure premixed laminar flames of methyl pentanoate/ O_2 /Ar and methyl hexanoate/ O_2 /Ar and atmospheric pressure flames of methyl pentanoate, each at stoichiometric and fuel-rich conditions, combined with computed results for each of these flames. A variety of reactant, intermediate, and product species mole fractions were measured in each flame. The specific operating conditions were chosen to study variations in flame structure due to differences in pressure, equivalence ratio, and fuel size.

2 Experiments

New experimental data were obtained on the structure of burner-stabilized flames of methyl pentanoate (MPe) and methyl hexanoate (MHe). Flames for both methyl esters were examined at low pressure conditions (20 Torr) at stoichiometric and rich equivalence ratios (φ), using a time-of-flight mass spectrometer with molecular beam flame sampling system and with photoionization by tunable vacuum ultraviolet (VUV) synchrotron radiation generated at the Advanced Light Source (ALS) of Lawrence Berkeley National Laboratory. Details on the experimental techniques used at the ALS have been presented in detail in previous publications [29–31]. The structures of atmospheric-pressure, stoichiometric and rich flames of MPe were studied in Novosibirsk by molecular beam mass spectrometry with soft ionization by electron impact and gas chromatography mass spectrometry [32–35]. Spectroscopic information for the major species and intermediates are summarized in Table S1 in the Supplementary Materials. Experimental mole fraction profiles of reactants, major flame products and many intermediates were obtained in each flame studied. All of the measured mole fractions in each flame are included as Table S2 in the Supplementary Materials.

Basic parameters of the six flames in this study are given in Table 1, and all of the experimental species measurements are included as Supplementary Material. Each flame is identified in Table 1 by a Flame Number FL# for discussion below. Figure 1 shows profiles of mole fractions of the major compounds in Flames 1 and 2 of MPe ($\varphi = 1$ and 1.5) at a pressure of 20 Torr, Flames 3 and 4 for MHe ($\varphi = 1$ and 1.3), also at 20 Torr, and Flames 5 and 6 for MPe ($\varphi = 1$ and 1.5) at atmospheric pressure, together with calculated values which will be discussed below. The overall features of all six flames are quite similar, with water as the largest product and the ratio of CO/CO₂ in the products depending on the overall fuel/oxidizer ratio. These profiles show that the widths of the combustion zone in all of the low pressure flames are about 7 mm and about 0.7–1.0 mm in the atmospheric pressure

Table 1: Ester flame conditions.

FL #	Fuel	Fuel	O ₂	Ar	P, Torr	phi	V, cm s ⁻¹
1	MPe	5.6	44.4	50	20	1.0	72.1
2		7.9	42.1	50	20	1.5	72.1
5		2.3	17.7	80	760	1.0	12.5
6		4.7	25.1	70.2	760	1.5	7.6
3	MHe	3.8	36.2	60	20	1.0	72.1
4		4.8	35.2	60	20	1.3	60.0

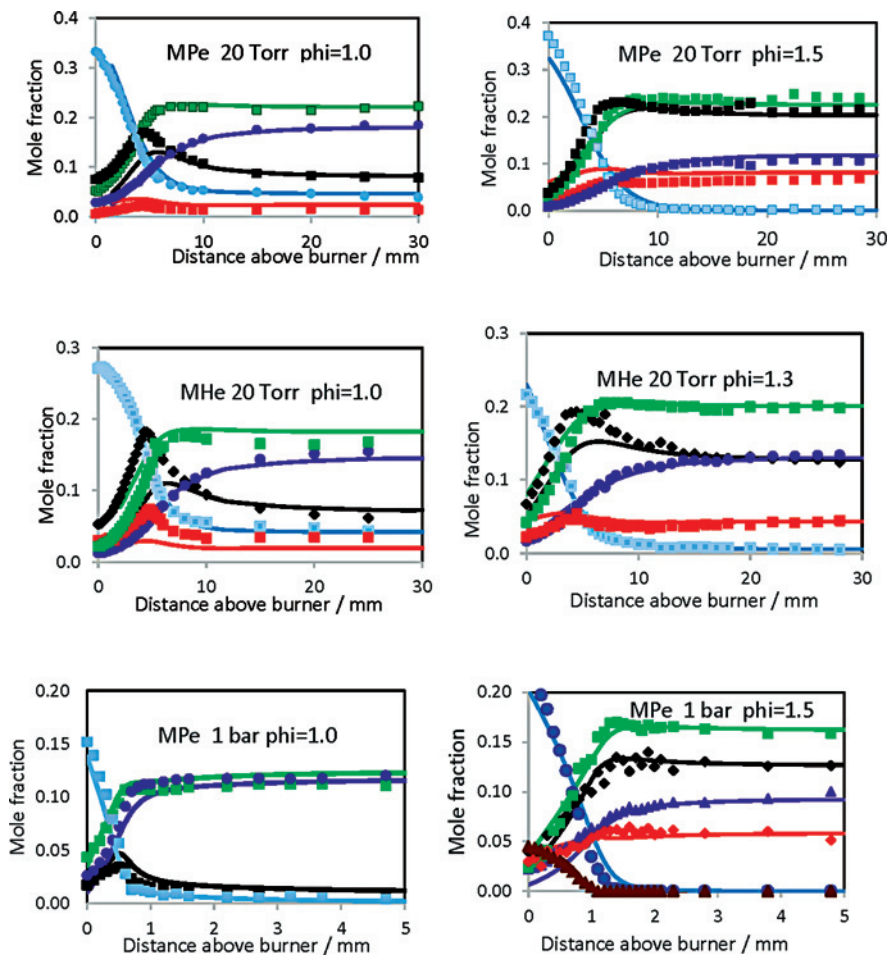


Figure 1: Major species in all six flames. Points are experimental results, lines are model calculations. Blue is O_2 , green is H_2O , purple is CO_2 , red is H_2 , black is CO , brown is fuel.

flames, and most of the chemistry in the post-flame gases is the approach to final equilibrium, which depends primarily on the overall equivalence ratio. Thus the equilibrium concentrations for the stoichiometric low pressure Flames 1 and 3 are very nearly identical, while the only significant difference between the final compositions in the rich, low pressure Flames 2 and 4 is the higher level of CO in the methyl pentanoate flame, due to its higher equivalence ratio ($\varphi = 1.5$) compared to the methyl hexanoate flame ($\varphi = 1.3$). The effect of pressure on equilibrium composition can be seen in Figure 1, comparing Flame 1 with Flame 5 and Flame 2 with Flame 6, where the primary differences between the product levels in the methyl

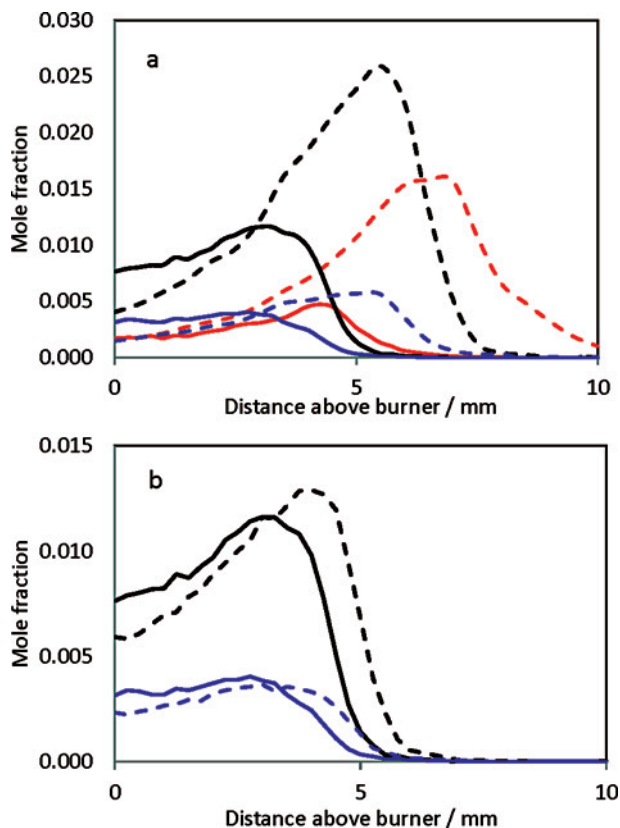


Figure 2: (a) Experimental C_2H_4 (black), C_2H_2 (red), and CH_2O (blue) mole fractions in Flame 1 (solid curves, MPe, $\varphi = 1.0$) and Flame 2 (dashed curves, MPe, $\varphi = 1.5$). (b) Experimental C_2H_4 (black) and CH_2O (blue) mole fractions in Flame 1 (solid curves, MPe, $\varphi = 1.0$) and Flame 3 (dashed curves, MHe, $\varphi = 1.0$).

pentanoate flames at both 20 Torr and 1 bar are the greater conversions of CO to CO_2 at the higher pressure.

In addition to the major species shown in Figure 1, in some or all of the flames the following intermediates were identified and their mole fraction profiles measured: methyl radical, methane, acetylene, ethene, formaldehyde, methanol, propyne, ketene, propene, acetaldehyde, vinylacetylene, 1,3-butadiene, 2-butene, 1-butene, propylene oxide, methyl propenoate, and methyl 3-butenate. Mole fractions of these compounds, as expected, differ from the stoichiometric to the fuel-rich flames. For example, in the stoichiometric flames, mole fraction profiles were measured for acetone, acetic acid, n-butanal and methyl propionate, while

the mole fractions of allene and methyl formate were measured only in the rich flames.

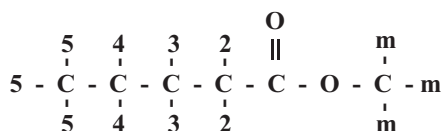
The detection limit of the facility used for the atmospheric pressure flames is not as precise as that used for the low pressure flames, so fewer intermediates were detected at atmospheric pressure, and only 11 intermediate species, CH_3 , CH_4 , C_2H_2 , C_2H_4 , C_3H_4 , 1,3-butadiene, 1-butene, methylpropenoate (methyl acrylate), methyl propanoate (methyl propionate), and methyl 3-butenolate were measured in the atmospheric pressure flames.

Spatial intermediate species concentrations measured experimentally for C_2H_4 , C_2H_2 and CH_2O are shown for the stoichiometric and rich methyl pentanoate Flames 1 and 2 in Figure 2a, illustrating the effects of increasing the fuel/oxidizer equivalence ratio. Increasing the equivalence ratio from 1.0 to 1.5 moves the flame farther away from the burner and increases the ethene and acetylene levels much more than it increases the formaldehyde levels. In Figure 2b, mole fractions of C_2H_4 and CH_2O are plotted for Flames 1 and 3, illustrating how similar these levels are in the methyl pentanoate and methyl hexanoate flames at the same pressure (20 Torr) and equivalence ratio ($\varphi = 1.0$). The key roles played in the oxidation of these fuels by C_2H_4 , C_2H_2 and CH_2O are discussed in the next section. Many other intermediate species show the same degree of similarity as that in Figure 2b for the flames of these two fuels, which is an important observation with implications for many other methyl ester fuel flames.

3 Kinetic modeling

Previous kinetic mechanisms used for simulations of low pressure premixed laminar flames of smaller alkyl esters were used as a base model for the present fuels. The most recent small hydrocarbon mechanism from NUI Galway [36] was used to update the C_0 – C_4 species core kinetic reaction mechanism and new high temperature reactions were added for consumption of methyl pentanoate and hexanoate and their immediate product species. For the most part, the mechanism additions consisted of adding one and two new CH_2 groups to an existing methyl butanoate mechanism [17], along with the corresponding decomposition reactions of the new fuel and its major radical species. Preliminary modeling tests were carried out to see if low T kinetics were likely to play any part in the flame structure calculations, and based on these assessments, no low T kinetic submodels were included for the present study. The entire reaction mechanism is provided as Table 3 in the Supplemental Material, but we will discuss the kinetic features that are unique to these methyl ester fuels.

Methyl pentanoate can be written schematically:



where ‘m’, ‘2’, ‘3’, ‘4’ and ‘5’ denote logically distinct H atoms in the methyl ester molecule. The structure of methyl hexanoate is the same, except the H atom sites are counted from ‘m’ to ‘6’, including one additional secondary methylene group. H atom abstraction reactions from the ‘3’ and ‘4’ (and ‘5’ for MHe) sites were assumed to have the same rates as for abstractions from secondary sites in common hydrocarbon fuels, and abstractions from the methoxy group (site ‘m’) and from the ‘5’ site (the ‘6’ site in MHe) were assumed to have conventional primary site abstraction rates. The C-H bond at the ‘2’ site is weaker than at conventional secondary C-H sites, due to electron delocalization from the oxygenated group in these alkyl ester fuels [37], and we assumed that the abstraction rates of H atoms at the ‘2’ site would be approximately equal to rates of abstractions from tertiary sites in conventional hydrocarbon molecules. As a result, H atom abstractions from the ‘2’ site are the fastest reactions of both of these fuels. The primary radicals in MPe and MHe decompose primarily via β -scission, with rates comparable to those in conventional hydrocarbon fuels.

Radical isomerization reactions via H atom transfer within these radicals were included in the mechanisms, using the same dependence of the reaction rates on the C-H bond being broken and the size of the transition state ring involved in the H atom transfer as those used in familiar hydrocarbon radicals [38]. The effects of the methyl ester group on isomerization rates, except for the involvement in the number of heavy atoms in the transition state ring, have been neglected, based on recent studies of Dibble [39] in larger methyl ester molecules.

Initiation reactions breaking C-C bonds as well as the C-O bonds in the methyl ester group that produce methyl or methoxy radicals have been included, as well as molecular elimination reactions [40], but initiation reactions do not contribute much to fuel consumption under laminar flame conditions, since nearly all fuel consumption is accomplished via H atom abstraction by fuel radicals.

4 Results

The six laminar premixed flames were modeled using the present kinetic reaction mechanism, using the Chemkin Pro burner stabilized laminar flame software [41]. Experimentally measured temperature profiles were used as input, and the energy equation was not solved. Each flame reached a solution with approximately 240 spatial points in the flame, and the computed chemical species mole fractions were computed and compared with the experimental results. Computed major species profiles for O_2 , CO , CO_2 , H_2 , and H_2O are compared with experimental values in Figure 1 for all six flames. Fuel mole fractions were also measured in each flame, although the results are shown in Figure 1 only for the rich, atmospheric pressure MPe flame. Fuel consumption is complete for each of the fuels at small distances from the burner. The overall agreement is excellent, with only the peak computed CO mole fractions somewhat smaller than the measured values for both low pressure MHe flames and the stoichiometric low pressure MPe flame. All of the major species mole fractions agree very well at distances far from the burner.

For each of the flames summarized in Table 1, selected computed mole fractions for intermediate species are compared with experimentally measured values in Figs. 3–8. For the low pressure flames, eight species comparisons are provided, including in each case CH_2O , CH_3 , CH_4 , C_2H_2 and C_2H_4 . In addition, three other species are shown for each flame, with combinations of oxygenated and methyl ester intermediates and some alkyne species. In all of the flames except Flame 2, the fuel-rich methyl pentanoate low pressure flame, methyl 2-pentenoate (MP2D) was measured experimentally and comparisons with computed values are shown.

A detailed reaction flux diagram for the methyl pentanoate flames is shown in Figure 9, combining results for the two low-pressure methyl pentanoate flames. In this complex figure, reaction fluxes for consumption of MPe and its products are shown for each reaction. Each branch is shown with two values, representing percentages of the total integrated rate of consumption of methyl pentanoate at equivalence ratios of 1.0 and 1.5, respectively. Since methylpentanoate is consumed completely in the flames, these values indicate percentages of parent fuel converted to the corresponding products in a particular reaction pathway. For example, the value “53.6” in the lower left-hand side of the figure indicates that in the stoichiometric flame, 53.6% of the fuel is eventually converted to $C_2H_5 + MP2D$.

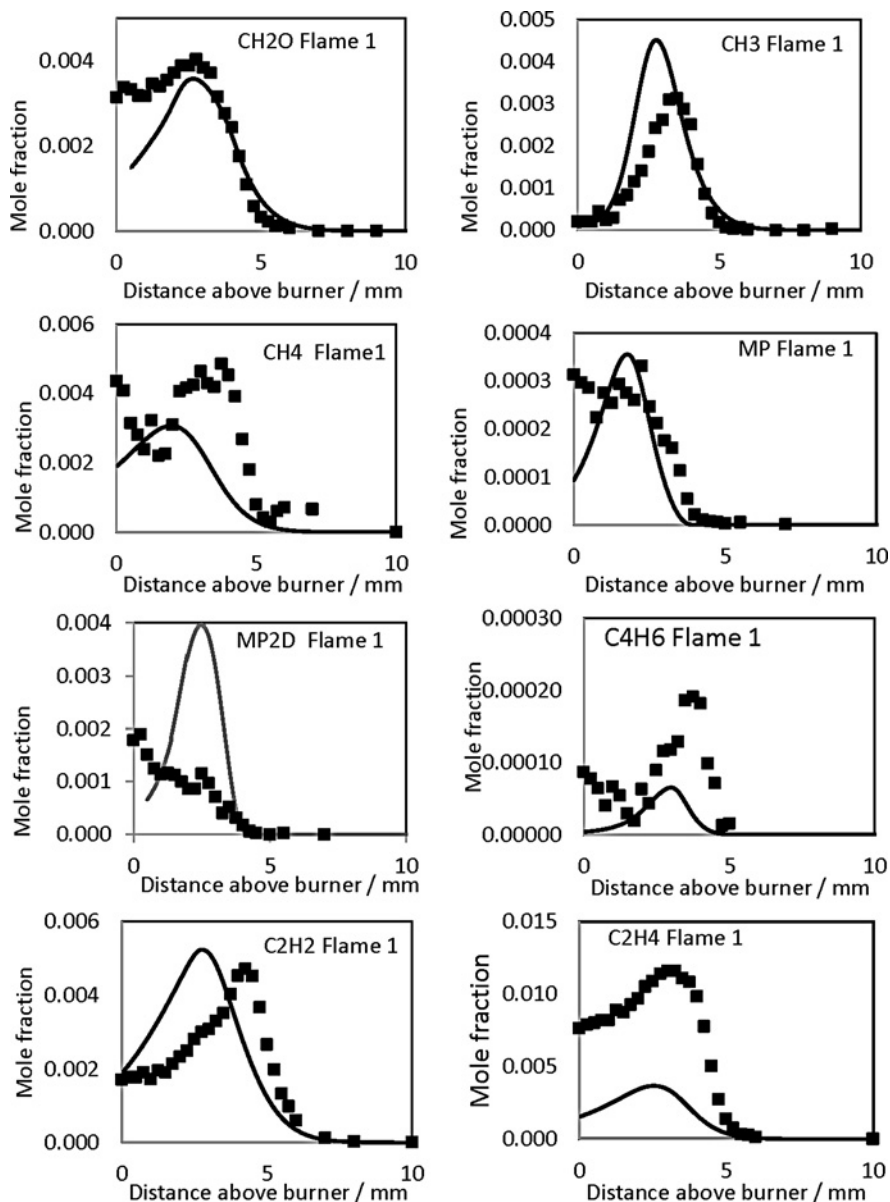


Figure 3: Experimental (symbols) and computed (lines) mole fractions for selected species in low pressure (20 Torr) stoichiometric ($\varphi = 1.0$) methyl pentanoate flame.

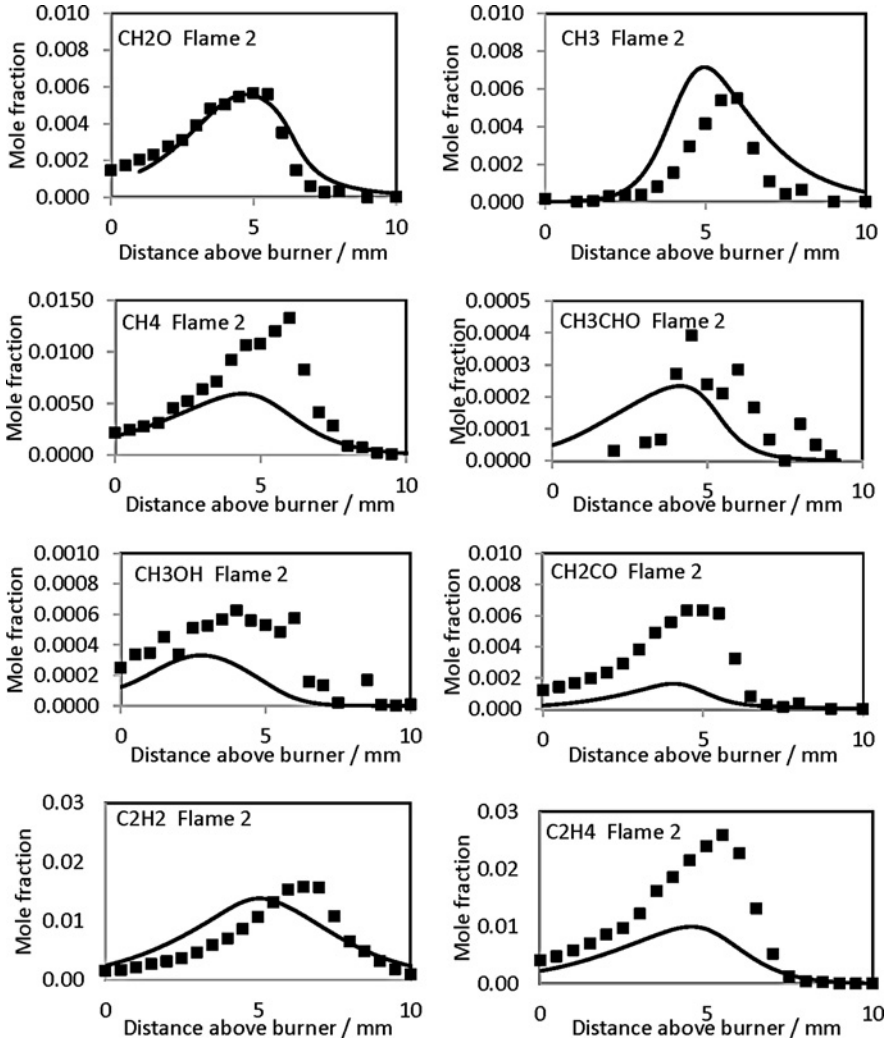


Figure 4: Experimental (symbols) and computed (lines) mole fractions for selected species in low pressure (20 Torr) fuel-rich ($\varphi = 1.5$) methyl pentanoate flame.

Integrated reaction rate was calculated in the same way as was done in [40]:

$$\omega_i = \int_0^{\infty} \omega'_i dt = \int_0^{\infty} \frac{\omega'_i}{v} dx$$

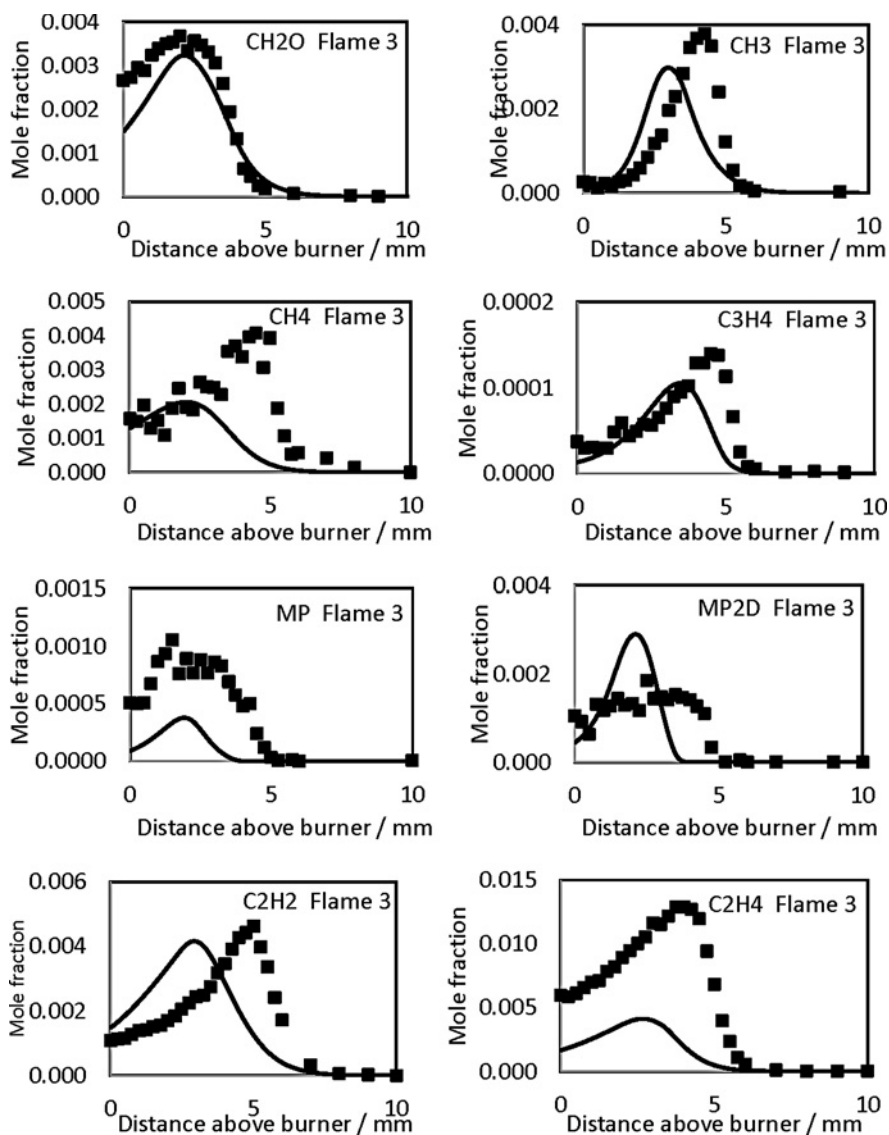


Figure 5: Experimental (symbols) and computed (lines) mole fractions for selected species in low pressure (20 Torr) stoichiometric ($\varphi = 1.0$) methyl hexanoate flame.

where ω'_i – local reaction rate i ($\text{mol}/(\text{cm}^3 \text{ s})$), v – local gas velocity (cm/s), x – distance from the burner (integration is carried out over the entire area of the flame). To calculate total integrated rate of consumption of methyl pentanoate, the summation was performed over all possible reactions associated with methyl

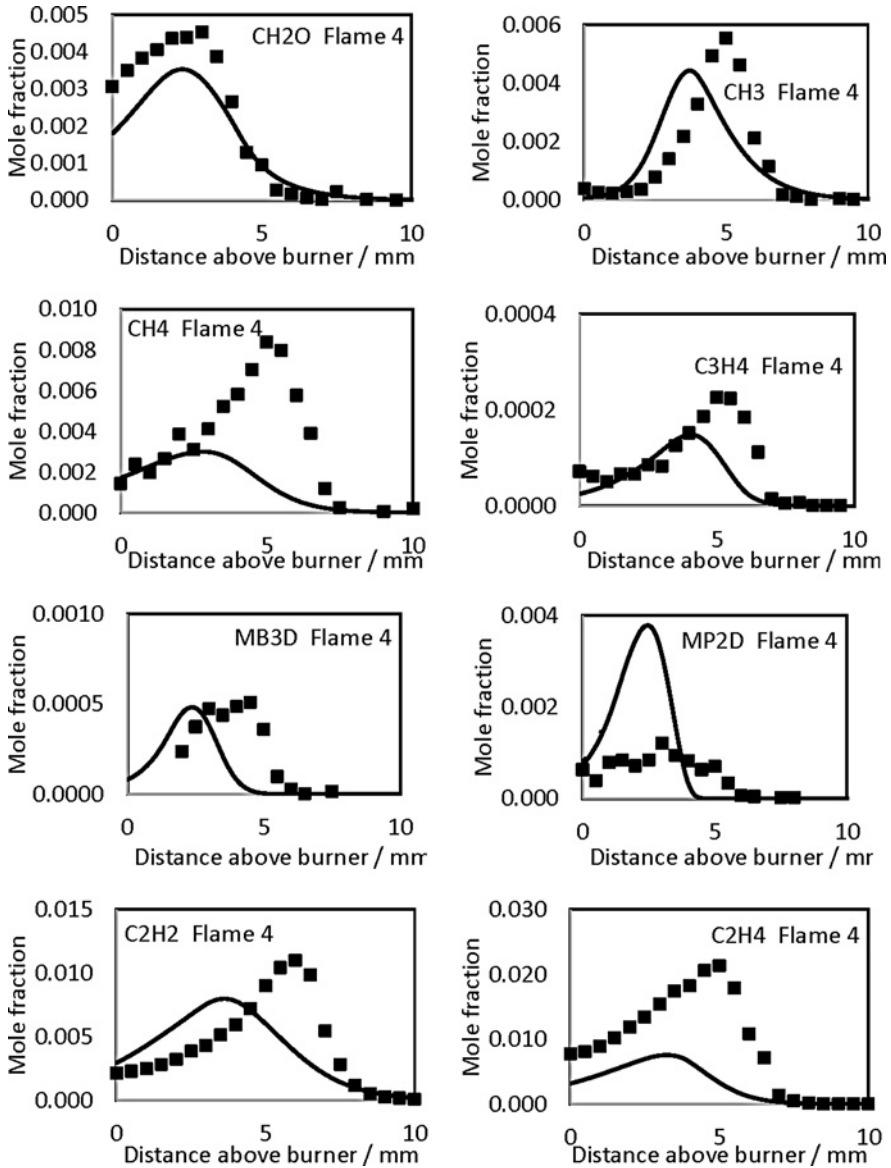


Figure 6: Experimental (symbols) and computed (lines) mole fractions for selected species in low pressure (20 Torr) fuel-rich ($\varphi = 1.3$) methyl hexanoate flame.

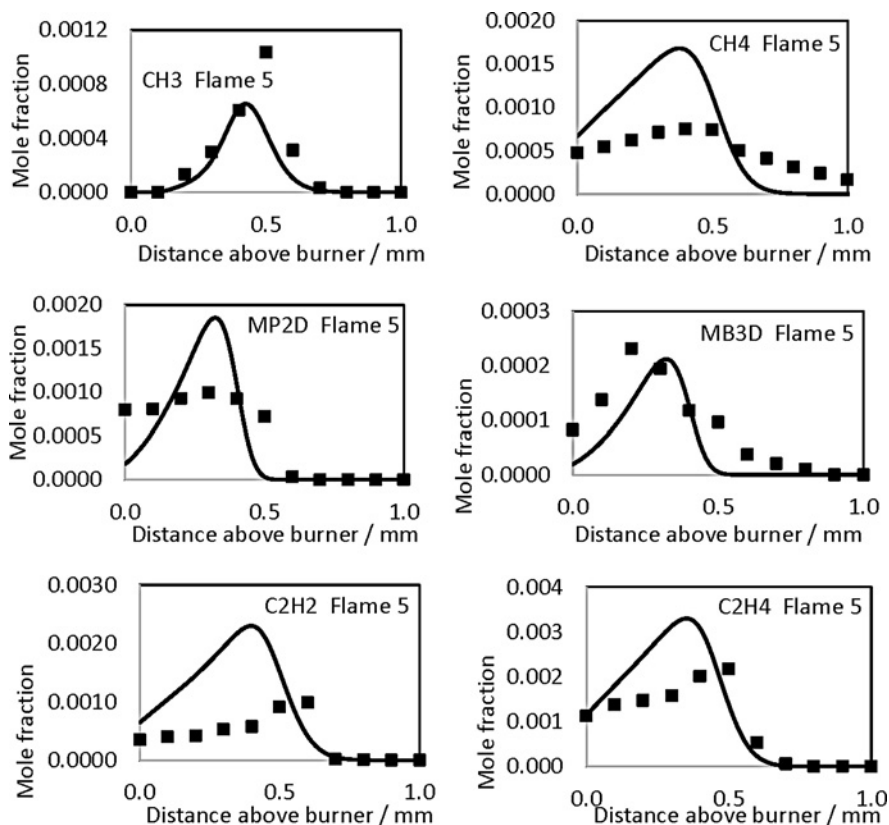


Figure 7: Experimental (symbols) and computed (lines) mole fractions for selected species in atmospheric pressure stoichiometric ($\varphi = 1.0$) methyl pentanoate flame.

pentanoate consumption. Very similar reaction fluxes were also obtained for methyl pentanoate flames at atmospheric pressure, so they are not included in this figure.

One important conclusion from the details in Figure 9 is that the same reaction pathways play very similar roles in all of the flames. In both flames, H atom abstraction is the only process consuming a significant fraction of the fuel, with the largest contribution ($\sim 40\%$) consistently from abstraction at the '2' site, and approximately equal contributions ($\sim 20\%$ each) from the secondary C-H '3' and '4' (and '5' in MHe) sites. The resulting radicals are consumed largely by β -scission. Not shown in Figure 9 is the fact that the major abstracting radical in the stoichiometric flame is OH, while the major abstracting radical in the rich flame is H. The same is true in all six flames we examined, and for both fuels and

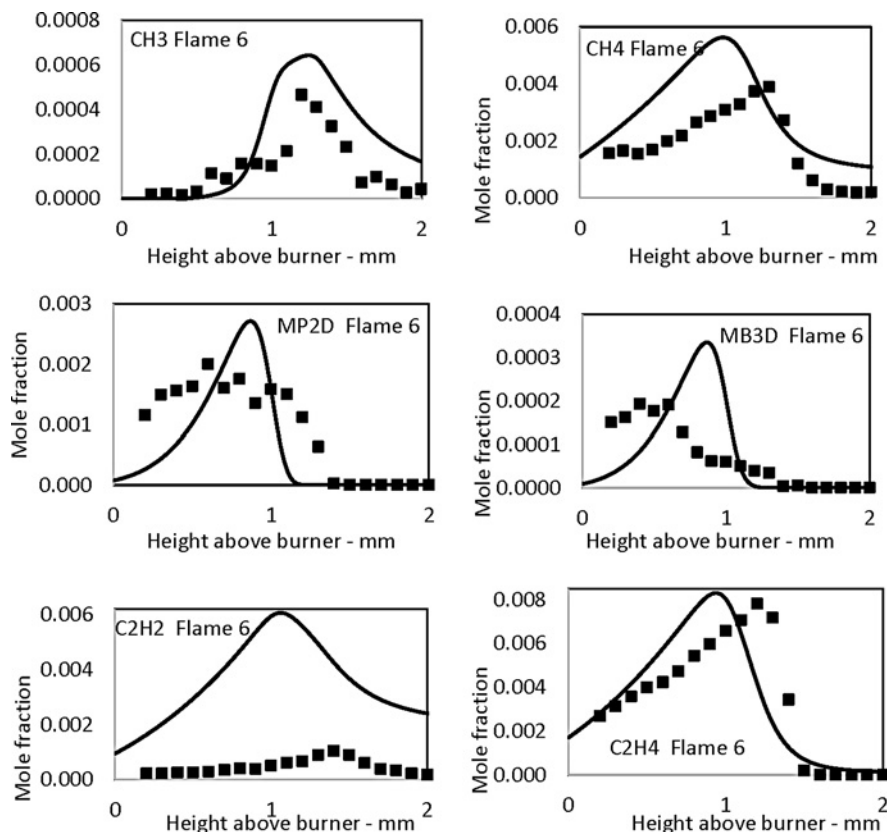


Figure 8: Experimental (symbols) and computed (lines) mole fractions for selected species in atmospheric pressure fuel-rich ($\varphi = 1.5$) methyl pentanoate flame.

for both of the pressures examined, H atom abstraction from the ‘2’ location has the highest overall rate.

Isomerization among the MPe radicals makes a minor contribution to consumption rates of most of these radicals, but isomerization reactions of the ‘m’-methyl pentanoate, the ‘4’-methyl pentanoate, and the ‘5’-methyl pentanoate radicals can produce the more stable, resonantly stabilized ‘2’-methyl pentanoate radical and making the 2-radical even more dominant when added to the effect of the preferential H-atom abstraction at that site. Decomposition of this radical via β -scission produces MP2D and ethyl radicals and subsequently ethene. A similar diagram for methyl hexanoate is shown in Figure 10, and it is conceptually the same as the diagram for methyl pentanoate in Figure 9; H atom abstraction from the fuel with the largest rate of abstraction occurring at the ‘2’ site, followed by β -

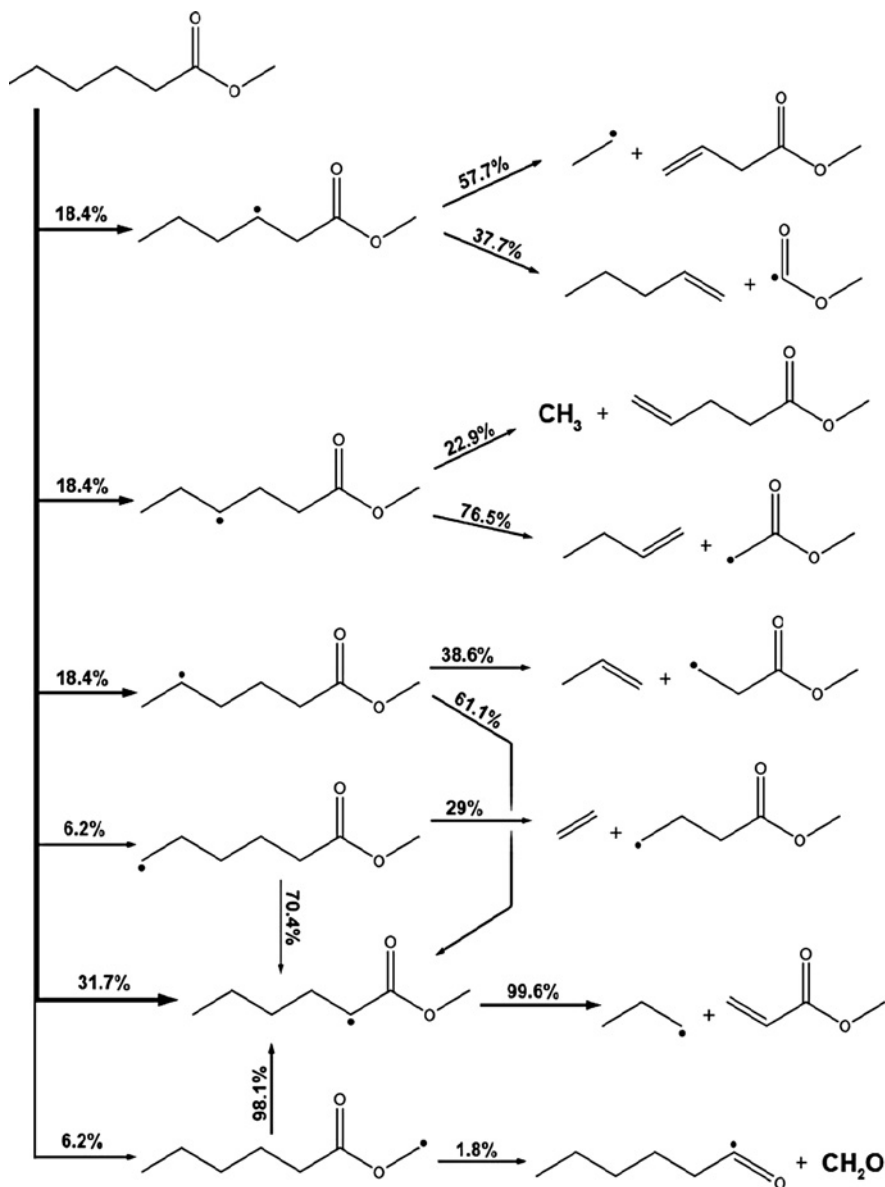


Figure 10: Reaction flux diagram for methyl hexanoate flames at 20 Torr. Values are percent conversions of each species being consumed.

Sequential decomposition of the methyl ester radicals also produces significant amounts of CO_2 at relatively early stages in the overall reaction. This is not commonly seen during oxidation of conventional hydrocarbons, where the majority of CO_2 production is delayed until most or all fuel and hydrocarbon intermediates have been consumed and radical levels can increase to convert CO to CO_2 . Most of the early CO_2 produced by alkyl ester reactions leading to decomposition of CH_3OCO [19–23]. This feature is important because production of early CO_2 by methyl esters limits the ability of methyl esters to reduce soot production in diesel combustion compared to other oxygenated hydrocarbon fuels [42].

Turning back to the detailed comparisons between computed and experimentally measured species in Figs. 3–8, there are a number of general observations that can be made. Overall, the agreement is quite good; this is particularly true of major intermediates including formaldehyde (CH_2O), methyl (CH_3) radicals, and, except for the rich, atmospheric Flame 6, acetylene (C_2H_2). There is good reason to question the experimental C_2H_2 results in Flame 6, which have maximum values of much less than 0.001 mole fraction, while the peak experimental ethene mole fraction in the same flame is close to 0.008. In all the other flames, peak experimental levels of C_2H_2 are approximately half the peak levels of C_2H_4 , so the C_2H_2 level in Flame 6 is unexpectedly low. In addition, for the 3 pairs of flames with common fuel and pressure but with one stoichiometric flame and one fuel-rich flame (i.e., Flame 1 and Flame 2; Flame 3 and Flame 4; Flame 5 and Flame 6), the measured C_2H_2 level increases by a factor of more than 3 from Flame 1 to Flame 2, the C_2H_2 level increases by a factor of more than 2 from Flame 3 to Flame 4, but the measured C_2H_2 level in Flame 6 is equal to the peak level in Flame 5, although the equivalence ratio of Flame 6 is 1.5 compared to the stoichiometric ratio in Flame 5, so the experimental values of C_2H_2 in Flame 6 may be too low.

Computed ethene mole fractions are lower than experimentally measured levels for all of the low pressure flames but show good agreement for the atmospheric pressure flames. We examined the kinetic model for possible additional reaction pathways to produce more ethene but did not identify any such reactions. Large increases in the rates of $\text{CH}_3 + \text{CH}_3$ reactions, even rates far outside of the accepted values, did not produce significantly higher levels of ethene in these flames. The same behavior has been observed in previous studies of low pressure laminar premixed flames [16–18] in which ethene mole fractions were measured using the same diagnostics as those used in the present study. We have commented previously that these discrepancies may arise from uncertainties in the photoionization cross sections for H_2O or C_2H_2 at 13.2 eV, which are used to determine the mole fractions for C_2 species. Alternatively, although we have included pressure dependence of the methyl recombination reactions in the present

kinetic reaction mechanism, further study of pressure dependence of these reactions is needed.

The reaction sequences in the present kinetic model that proceeds via decompositions of the 2-methyl pentanoate and 2-methyl hexanoate radicals yield approximately equal amounts of ethene and MP2D, and the computed levels of ethene and MP2D are roughly equal in all four of the low pressure flames summarized in Figs. 3–6 and in the stoichiometric atmospheric flame shown in Figure 7. For the rich atmospheric flame shown in Figure 8, methyl recombination produces additional amounts of C_2 species and the ethene levels in that flame are 2–3 times larger than the MP2D levels. However, in the low pressure flames, the experimentally measured levels of ethene are greater than the measured MP2D levels by factors of 6–15, seriously inconsistent with the computed trends. Further study of the photoionization cross sections for ethene and MP2D and pressure dependence of the methyl recombination reactions are needed to resolve these differences.

Both experiments and computations show that the major ester intermediate is methyl 2-propenoate (MP2D), and modeling results seem to agree quite well with measured values for those flames in which it was measured. The computed results show MP2D as a smooth curve with a defined peak and width slightly less than the full flame width. Since MP2D is a species closely associated with fuel consumption, this type of spatial variation seems appropriate, but the experimental results show a much less peaked shape than the calculated values. The experimental measurements suggest a flame that extends back into the burner region where measurements are effectively impossible, while the computations suggest a well-defined flame centered off the surface of the burner. The level of agreement between model and experiment for MP2D is probably best characterized as being as good as can be expected, given that the order of magnitude of the mole fractions agree quite well, and better agreement is not possible.

For many of the species spatial profiles in Figs. 3–8, there appears to be a difference in the locations of the peak values of mole fractions of about 1 mm, with many of the computed results reaching their peaks closer to the burner than the experimental peaks. Many studies in the past have included extended discussions of why it is appropriate to shift either the experimental or the computed species profiles in either direction. We have chosen to present both the experimental and computed results without modification. Indeed, for most of these flames, some but not all of the profiles in Figs. 3–8 show some offset. For Flame 1 in Figure 3, the CH_2O curves agree very closely without any spatial shift to either the experimental or computed profile, while the C_2H_2 curves seem to be nearly identical but offset by about 1 mm. In fact, for Flames 1–4, the same trend is easily recognized. From careful examination of both the computed and experimental results, no obvious resolution is obvious. The only trend we observed was that the

atmospheric flames appear to be, as a whole, better centered than the low pressure flames.

Another general observation is that, while the figures show generally good agreement between experimental and computed levels of CH_3 , the computed CH_4 profiles are consistently smaller than the experimental values for the low pressure flames. The experimental uncertainties of the CH_4 measurements are smaller than the disagreements with the computed results, so we have concluded that model corrections are indicated. This disagreement is not seen in the atmospheric pressure flames, and since methane is not a direct product of the experiments but is produced via reactions of the methyl radicals, the pressure dependence of recombination reactions involving methyl radicals and H atoms is likely responsible, and further attention to these rates and thermochemistry is needed.

5 Conclusions

The present results provide new experimental data from premixed laminar flame experiments for two methyl ester fuels, methyl pentanoate and methyl hexanoate, experiments in which a large number of intermediate species mole fractions have been measured. The kinetic model developed to simulate these flames has provided predictions of major and many other species mole fractions with good accuracy, although some refinements are still needed. The kinetic mechanisms for methyl pentanoate and methyl hexanoate were constructed based on current model parameters for other fuels, and no mechanism refinements were made subsequent to the initial model production. As a result, extensions of the same approach to larger and more complex alkyl ester fuels should be possible with considerable confidence. In this sense, kinetic reaction mechanisms for methyl esters have reached the same level of maturity as those for conventional hydrocarbon fuels. Together with other recent studies of other methyl ester fuels in the size range from methyl pentanoate to methyl octanoate, a collective capability has been provided for kinetic modeling of these fuel families, including previously challenging spatially varying problems such as laminar flames. However, kinetic models still have many unsolved problems for both alkyl ester and conventional hydrocarbon fuels, including uncertainties for low temperature reaction pathways and for fuels that have single and multiple C=C double bonds, where many kinetic features involving these double bonds still need considerably more attention.

Acknowledgement: The experimental work was supported by RFBR under grant #11-03-92503; CRDF under grant #RUC2-7027-NO-11; and the Ministry of Educa-

tion and Science of the Russian Federation under project No. 8186. Experimental and computational work was supported by the US Department of Energy, Office of Vehicle Technologies and the Office of Basic Energy Sciences and was performed under the auspices of the US Department of Energy under Contract DE-AC52-07NA27344 by the Lawrence Livermore National Laboratory (CKW) and under Contract DE-AC04-94-AL85000 by the Sandia Corporation (NH). The Advanced Light Source is supported by the Director, Office of Science, BES/USDOE under Contract No. DE-AC02-05CH11231.

References

1. M. S. Graboske and R. L. McCormick, *Prog. Energ. Combust.* **24** (1998) 125.
2. K. Kohse-Hoinghaus, P. Oswald, T. A. Cool, T. Kasper, N. Hansen, F. Qi, C. K. Westbrook, and P. R. Westmoreland, *Angew. Chem. Int. Ed.* **49** (2010) 3572.
3. C. K. Westbrook, *Annu. Rev. Phys. Chem.* **64** (2013) 201.
4. M. Lapuerta, O. Armas, and A. Rodriguez-Fernandez, *Prog. Energ. Combust.* **34** (2008) 198.
5. C. J. Mueller, A. L. Boehman, and G. C. Martin, SAE-2009-01-1792., *Soc. Auto. Eng., Warrendale, PA, USA*, (2009).
6. C. K. Westbrook, C. V. Naik, O. Herbinet, W. J. Pitz, M. Mehl, S. M. Sarathy, and H. J. Curran, *Combust. Flame* **158** (2011) 742.
7. C. V. Naik, C. K. Westbrook, O. Herbinet, W. J. Pitz, and M. Mehl, *P. Combust. Inst.* **33** (2011) 383.
8. C. K. Westbrook, W. J. Pitz, S. M. Sarathy, and M. Mehl, *P. Combust. Inst.* **34** (2013) 3049.
9. P. Dagaut, S. Gail, and M. Sahasrabudhe, *P. Combust. Inst.* **31** (2007) 2955.
10. S. Bax, M. H. Hakka, P.-A. Glaude, and O. Herbinet, *Combust. Flame* **157** (2010) 1220.
11. M. H. Hakka, P. A. Glaude, O. Herbinet, and F. Battin-Leclerc, *Combust. Flame* **156** (2009) 2129.
12. O. Herbinet, W. J. Pitz, and C. K. Westbrook, *Combust. Flame* **154** (2008) 507.
13. O. Herbinet, W. J. Pitz, and C. K. Westbrook, *Combust. Flame* **157** (2010) 893.
14. M. F. Campbell, D. F. Davidson, R. K. Hanson, and C. K. Westbrook, *P. Combust. Inst.* **34** (2013) 419.
15. O. Herbinet, J. Biet, M. H. Hakka, V. Warth, P.-A. Glaude, A. Nicolle, and F. Battin-Leclerc, *P. Combust. Inst.* **33** (2011) 391.
16. S. Dooley, F. L. Dryer, B. Yang, J. Wang, T. A. Cool, T. Kasper, and N. Hansen, *Combust. Flame* **158** (2011) 732.
17. B. Yang, C. K. Westbrook, T. A. Cool, N. Hansen, and K. Kohse-Hoinghaus, *Phys. Chem. Chem. Phys.* **13** (2011) 6901.
18. B. Yang, C. K. Westbrook, T. A. Cool, N. Hansen, and K. Kohse-Hoinghaus, *P. Combust. Inst.* **34** (2013) 443.
19. L. R. McCunn, K.-C. Lau, M. J. Krisch, and L. J. Butler, *J. Phys. Chem. A* **110** (2006) 1625.
20. P.-A. Glaude, W. J. Pitz, and M. J. Thomson, *P. Combust. Inst.* **30** (2005) 1111.
21. C. J. Hayes and D. R. Burgess Jr., *P. Combust. Inst.* **32** (2009) 263.
22. R. E. Weston, T. L. Nguyen, J. F. Stanton, and J. R. Barker, *J. Phys. Chem. A* **117** (2013) 821.

23. A. Farooq, D. F. Davidson, R. K. Hanson, L. K. Huynh, and A. Violi, *P. Combust. Inst.* **32** (2009) 247.
24. G. Dayma, S. Gaïl, and P. Dagaut, *Energ. Fuel.* **22** (2008) 1469.
25. G. Dayma, C. Togbé, and P. Dagaut, *Energ. Fuel.* **23** (2009) 4254.
26. G. Dayma, S. M. Sarathy, C. Togbe, C. Yeung, M. J. Thomson, and P. Dagaut, *P. Combust. Inst.* **33** (2011) 1037.
27. G. Dayma, F. Halter, F. Foucher, C. Mounaim-Rousselle, and P. Dagaut, *Energ. Fuel.* **26** (2012) 4735.
28. P.-A. Glaude, O. Herbinet, S. Bax, J. Biet, V. Warth, and F. Battin-Leclerc, *Combust. Flame* **157** (2010) 2035.
29. T. A. Cool, A. Mcllroy, F. Qi, P. Westmoreland, L. Poisson, D. S. Peterka, and M. Ahmed, *Rev. Sci. Instrum.* **76** (2005) 094102.
30. N. Hansen, T. A. Cool, P. R. Westmoreland, and K. Kohse-Hoinghaus, *Prog. Energ. Combust.* **35** (2009) 168.
31. T. A. Cool, K. Nakajima, C. A. Taatjes, A. Mcllroy, P. R. Westmoreland, M. E. Law, and A. Morel, *Proc. Combust. Sci.* **30** (2005) 1681.
32. O. P. Korobeinichev, S. B. Ilyin, V. V. Mokrushin, and A. G. Shmakov, *Combust. Sci. Technol.* **116-117** (1996) 51.
33. O. P. Korobeinichev, S. B. Ilyin, V. M. Shvartsberg, and A. A. Chernov, *Combust. Flame* **118** (1999) 718.
34. O. P. Korobeinichev, V. M. Shvartsberg, A. G. Shmakov, T. A. Bolshova, T. M. Jayaweera, C. F. Melius, W. J. Pitz, C. K. and Westbrook, *P. Combust. Inst.* **30** (2005) 2353.
35. T. M. Jayaweera, C. F. Melius, W. J. Pitz, C. K. Westbrook, O. P. Korobeinichev, V. M. Shvartsberg, A. G. Shmakov, I. V. Rybitskaya, and H. J. Curran, *Combust. Flame* **140** (2005) 103.
36. W. K. Metcalfe, S. M. Burke, S. S. Ahmed, and H. J. Curran, *Int. J. Chem. Kinet.* **45** (2013) 638.
37. A. M. El-Nahas, M. V. Navarro, J. M. Simmie, J. W. Bozzelli, H. J. Curran, S. Dooley, and W. Metcalfe, *J. Phys. Chem. A* **111** (2007) 3727.
38. H. J. Curran, P. Gaffuri, W. J. Pitz, and C. K. Westbrook, *Combust. Flame* **114** (1998) 149.
39. F. Zhang and T. S. Dibble, *J. Phys. Chem. A* **115** (2011) 655.
40. W. Metcalfe, P. Togbe, P. Dagaut, H. J. Curran, and J. M. Simmie, *Combust. Flame* **156** (2009) 250.
41. CHEMKIN-PRO 15112, Reaction Design, San Diego (2011).
42. C. K. Westbrook, W. J. Pitz, and H. J. Curran, *J. Phys. Chem. A* **110** (2006) 6912.

Supplementary material: The online version of this article (DOI: 10.1515/zpch-2014-0596) provides supplementary material for authorized users.